AERODYNAMIC ANALYSIS OF A WING-BODY CONFIGURATION IN SUPERSONIC FLOW

Gustavo Bono, bonogustavo@gmail.com
Federal University of Rio Grande do Sul,
Graduate Program in Mechanical Engineering,
Av. Sarmento Leite 425, 90050-170 Porto Alegre, RS,
Brazil

Armando M. Awruch, amawruch@ufrgs.br
Federal University of Rio Grande do Sul,
Applied and Computacional Mechanical Center,
Av. Osvaldo Aranha 99, 90035-190 Porto Alegre, RS,
Brazil

Abstract. *Euler and Navier-Stokes simulations are performed over a wing-body configuration in supersonic regime. The numerical analysis is carried out using the Finite Element Method with an explicit one-step Taylor-Galerkin scheme and adaptive unstructured meshes employing linear tetrahedral elements. The analysis focused different Mach numbers (M = 2.3 and 4.63) and angles of attack (alpha = 6.2º and 11.1º). Finally, the structure of the flow field is discussed for each case and computational results are compared to available experimental data.*

Keywords*: supersonic flow, finite element method, adaptive mesh strategy, wing-body configuration*

1. INTRODUCTION

Current and expected developments in space transportation have led to growing interest in new space vehicles. Several expendable and partially or fully reusable concepts are discussed or already planned. These new vehicles require essential improvements over current vehicles in order to ensure economic viability and to fulfill mission and safety constraints. A numerical investigation is conducted to determine the structure of the flow field and the main aerodynamic characteristics over a wing-body (W-B) configuration at high supersonic speeds. The wing-body configuration could be compared with some supersonic transport vehicles, aerospace vehicles, guided missiles or a generic Unmanned Combat Air Vehicle (UCAV).

The three-dimensional flow on the W-B configuration is complex and it contains a variety of interactions. To obtain an accurate solution, it is evident that considerable benefit could be achieved if the mesh employed is, in some way, adapted to the solution in an optimal manner. Adaptive meshing is a powerful tool in CFD that substantially enhances the accuracy, efficiency, and automation of the numerical methods. In this work, an adaptive mesh method is employed to enhance the definition of complex flow features over the W-B configuration.

The purpose of this paper is to report results of numerical tests analyzing the aerodynamic effects of inviscid and viscous flows about a wing-body configuration. A three-dimensional Euler/Navier-Stokes solver is used jointly with a spatial refinement technique. Simulations are performed for two supersonic Mach number and for two angles of attack. The accuracy of the computational techniques developed and applied in this study is demonstrated through comparison with available experimental data.

2. SOME REMARKS ABOUT THE NUMERICAL ALGORITHM

In this work, we will only be concerned with the solution of steady flows. These solutions will be achieved by advancing the time dependent governing equations until steady conditions are obtained. An explicit one-step scheme is employed for solving the compressible inviscid/viscous flow problems. The results presented in this paper have been obtained using an unstructured mesh with tetrahedral finite elements and the Euler as well as Navier-Stokes solvers, with a mesh refinement technique.

The one-step scheme is similar to that presented by Donea (1984). Applying Taylor expansion to the unknown variables in time and the classical Bubnov-Galerkin weighted residual technique in the context of the finite element method (FEM), the time-space discretisation is obtained. Finally equations are solved with an explicit scheme. More details can be found in Bono (2008). The explicit algorithm is subjected to the Courant-Friedrichs-Lewy stability criterion. At supersonic speeds, an additional numerical damping is necessary to capture strong shocks and to smooth local oscillations in the vicinity of these shocks. An artificial viscosity model, as proposed by Argyris *et al.* (1990), due to its simplicity and efficiency in terms of CPU time, is adopted here.

Numerically accurate and computationally efficient solutions may be obtained employing mesh adaptation techniques, because the mesh is only locally refined at the places of interest. An adaptive mesh strategy basically is characterized by an error indicator, an adaptive criterion and a refinement scheme. The error indicator is used to identify

the characteristics and behavior of the numerical solutions in order to determine regions of the computational domain where a refinement process is necessary, looking for an accurate solution. In this work, these error indicators take into account regions with low velocity components (LV), change in the direction of velocity components (DV), velocity gradients (VG), pressure gradients (PG) and specific mass gradients (RG). The criterion for mesh adaptation is based in the normal distribution of the error indicators and their mean values and standard deviation. The adaptive process was performed using the *h*-refinement method. Details of the error indicators, mesh adaptation and the refinement process can be found in Popiolek and Awruch (2006).

3. NUMERICAL RESULTS

In this section, results are presented for a wing-body (W-B) configuration for steady flows. Jernell (1971) obtained experimental results for a W-B configuration with varying Mach number (2.30 to 4.63) and different angles of attack (0º to 11.1º). The front of the fuselage is generated with the criteria of Haack (Jernell, 1971), which predicts the profile required to minimize the wave drag. The remaining aft section of the fuselage is cylindrical. The wing has a delta planform of 65º leading edge sweep and a symmetrical double-wedge airfoil of 6 percent thickness.

In this study, Euler and Navier-Stokes equations are used. Firstly, results obtained for an inviscid flow (WBeu) are presented and later on results obtained in viscous flow (WBns) with a free stream Reynolds number equal to Re = $1x10^5$ are shown. The different cases computed here are listed in Tab. 1. It should be noted that in both examples supersonic flows are considered.

Table 1. W-B cases computed in this example, where *eu* = inviscid flow and *ns* = viscous flow.

		Angle of attack (deg)	
		6.2	11.1
Mach	2.30	WBns3	WBeu1 WBns1
	4.63	WBeu2 WBns2	WBns4

The first simulations for all cases are performed using the same initial mesh consisting of 194501 tetrahedral elements. The identification of each example, the number of nodes (*nno*), the number of elements (*nele*), the number of nodes on the W-B configuration (*nnoCS*), the maximum edge length (L_{max}), the minimum edge length (L_{min}) and the minimum time step (Δt) are described in Tab. 2.

Table 2. Numerical parameters for the W-B configuration.

cases	mesh	*nno*	*nele*	*nnoCS*	L_{max}	L_{min}	Δt
M =2.30	WBns3	37061	194501	6877	8.08	$7.47x10^{-3}$	$2x10^{-4}$
α = 6.2º	WBns3R1	217212	1193165	27124	8.03	$3.73x10^{-3}$	$1x10^{-4}$
M =2.30 α =11.1º	WBeu1	37061	194501	6877	8.08	$7.47x10^{-3}$	$2x10^{-4}$
	WBeu1R1	118082	659121	10422	8.08	$3.73x10^{-3}$	$1x10^{-4}$
	WBeu1R2	364996	2093370	14635	8.08	$1.87x10^{-4}$	$5x10^{-5}$
	WBns1	37061	194501	6877	8.08	$7.47x10^{-3}$	$2x10^{-4}$
	WBns1R1	214427	1177222	27124	8.08	$3.73x10^{-3}$	$1x10^{-4}$
M =4.63 α = 6.2º	WBeu2	37061	194501	6877	8.08	$7.47x10^{-3}$	$1x10^{-4}$
	WBeu2R1	124897	697869	10906	8.08	$3.73x10^{-3}$	$1x10^{-4}$
	WBns2	37061	194501	6877	8.08	$7.47x10^{-3}$	$1x10^{-4}$
	WBns2R1	187406	1055245	13647	8.03	$4.69x10^{-3}$	$8x10^{-5}$
M= 4.63	WBns4	37061	194501	6877	8.08	$7.47x10^{-3}$	$1x10^{-4}$
α =11.1º	WBns4R1	185123	1044230	12864	8.03	$4.69x10^{-3}$	$8x10^{-5}$

The adaptive mesh technique is employed in all cases with the following errors indicators: VG, PG and RG for the inviscid cases and LV, DV, VG, PG and RG for the viscous cases. More details can be found in Bono (2008). The first and second refinements were identified as R1 and R2, respectively.

3.1. Inviscid cases

In Fig. 1, the specific mass distributions, obtained with the initial mesh (WBeu1) and final mesh (WBeu1R2) (using refinement levels in the cases of Mach number 2.30 and angle of attack 11.1 deg), are shown. Improvement in the definition of the principal flow features (expansion fan and shock wake) on the adapted mesh is clearly observed.

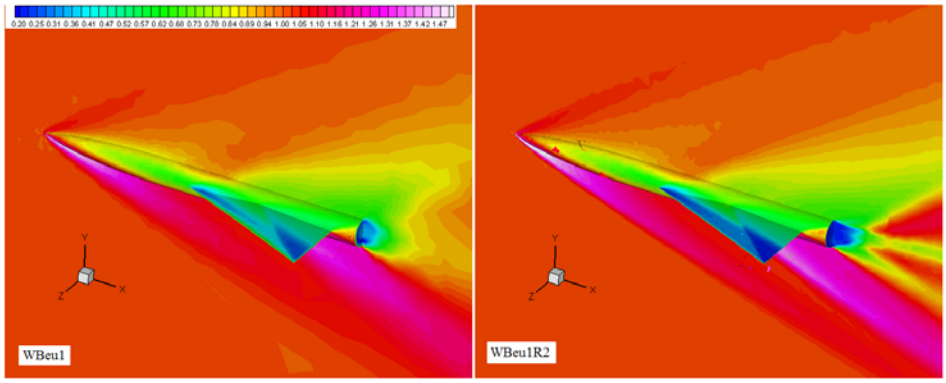

Figure 1. Specific mass contours for the initial (WBeu1) and final (WBeu1R2) meshes for M = 2.30 and α = 11.1º

Figure 2 shows Mach number distribution and meshes in the plane perpendicular to the W-B model centerline, for x_b/L = 0.80, where x_b is the axial distance, which is normalized with respect to the body length L. The flow expands around the leading edge onto the upper surface of the wing, forming of a relative weak shock at a position located at 70% of the semispan. The initial mesh is not able to capture the shock wave formed on the upper surface of the wing and on the lower part the W-B configuration.

The distribution of the pressure coefficient across the delta wing at two different locations ($2y/b$) across the span is compared with experimental results presented by Jernell (1971) in Fig. 3. Numerical results are obtained employing the final mesh. In the location, *2y/b*, *y* is the spanwise distance, normalized with respect to the semispan *b/2*. Excelent agreements between the experimental and numerical results with two refinement levels are obtained.

The pressure coefficient distribution at four different sections is shown in Figure 4 for the mesh with two refinement. The level of agreement between the numerical prediction and experimental results (Jernell, 1971) is certainly acceptable considering that only one refinement level is employed.

The specific mass distribution on the three views of the W-B configuration WBeu1R2 (M=2.30 and α=11.1º) and WBeu2 (M=4.63 and α=6.2º) are shown in Fig. 5. The letters U and L indicate upper and lower surfaces, respectively. The compression and expansion regions on the wing and body are clearly identified in both examples. The distribution on the body is strongly influenced by the wing-body intersection. On the lower surface of the wing, the specific mass is initially compressed (the specific mass increase) in the front of the wing due to the shock wave in the leading edge. After this region the flow expands through an expansion fan. In the front of the body the flow is more compressed in the mesh corresponding to the case WBeu2 with M = 4.63 than the mesh corresponding to the case WBeu1R2 with M = 2.30.

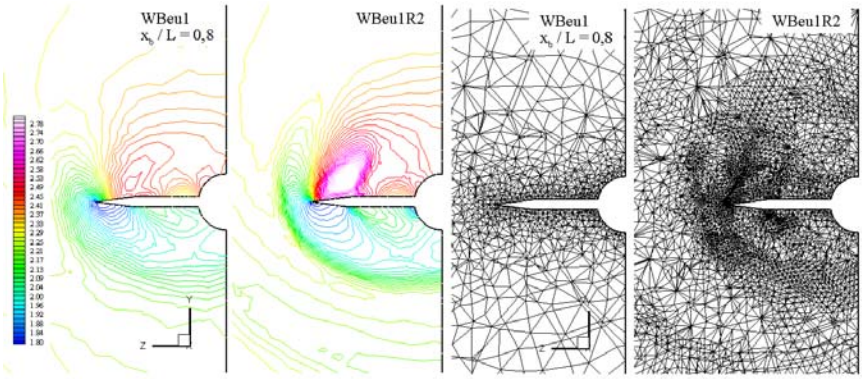

Figure 2. Mach number distribution and meshes in x_b/L = 0.80 for M = 2.30 and alpha = 11.1º

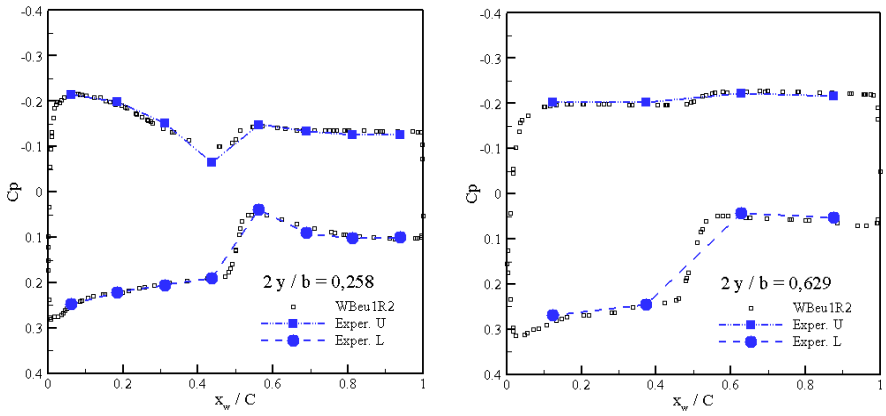

Figure 3. Pressure coefficient over a W-B configuration. Comparison between numerical prediction and an experimental work at different sections for the final mesh (WBeu1R2)

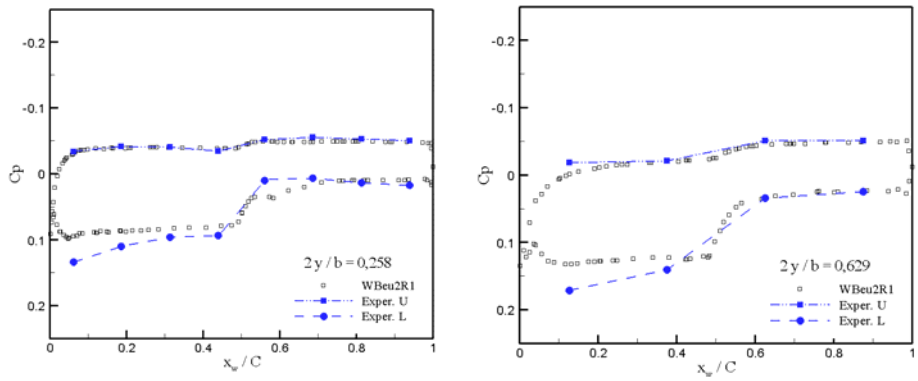

Figure 4. Pressure coefficient over a W-B configuration. Comparison between numerical prediction and an experimental work at different sections for the mesh with one refinement (WBeu2R1)

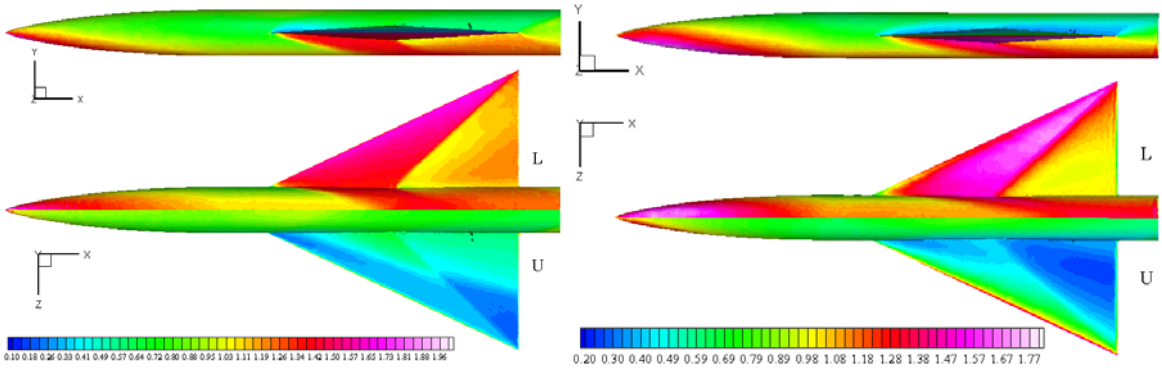

Figure 5. Specific mass distribution over a W-B configuration for WBeu1R2 (left) and WBeu2 (right)

The region with the minimum value of the specific mass is located on the upper surface and near the leading edge for the final mesh (WBeu1R2, M=2.30 and α=11.1º), however, for the initial mesh (M=4.63 and α=6.2º) the region with the minimum value of ρ is located approximately in the middle of the delta wing.

3.2. Viscous cases

The Mach number distribution over the W-B configuration for different stations (x_b/L=0.1 to 1.2 with steps equal to 0.1) are shown in Fig. 6 for all Mach number-angle of attack combinations (see Tab. 1). It should be noted that, in

regions with low speed, the Mach number is higher in cases where the angle of attack is equal to 11.1º compared to those with α=6.2º. The Mach number distribution in the upper region of the body with M = 4.63 shows some differences with respect to that obtained with M = 2.30.

The pressure coefficient (Cp) distribution, presented in Fig. 7, shows the influence of the Mach number and angle of attack for different stations (x/C_r) over the W-B configuration. The coordinate x is normalized with respect to the root chord C_r and the origin is located in the leading edge. As expected, the pressure coefficient increases with the angle of attack and growth is greater on the lower surface of the delta wing. The pressure coefficient is larger in the leading edge due to the detached shock wave.

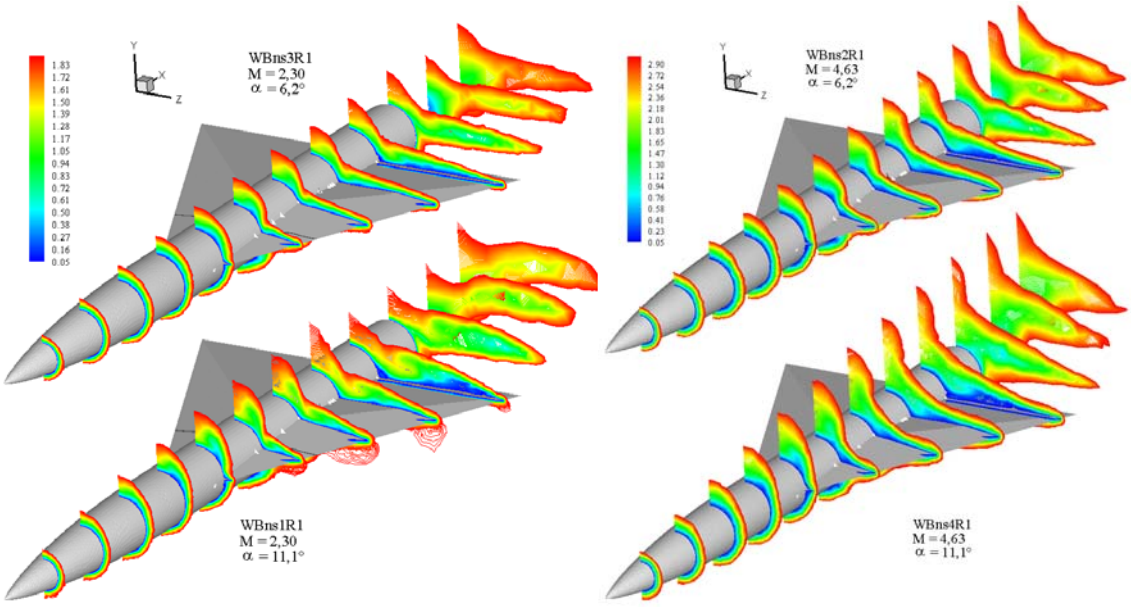

Figure 6. Mach number distribution over a W-B configuration for M=2.3 (left) and M=4.63 (right)

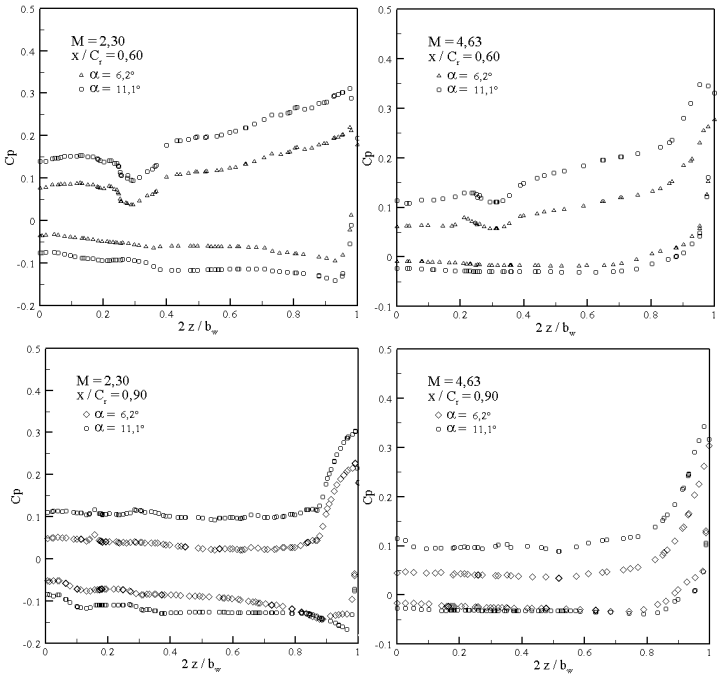

Figure 7. Pressure coefficient distribution over a W-B configuration for M=2.3 (left) and M=4.63 (right) with angle of attack 6.2º and 11.1º

On the lower surface of the wing (rear region) a reduction in the pressure coefficient is observed because the flow is accelerated by the expansion fan in the region of maximum thickness. It should be noted that for the same stations and

angles of attack the pressure coefficient is always lower for the higher Mach number. The reduction of Cp with the Mach number increase is in essence explained by the principle of independence of the Mach number.

The pressure coefficient distributions over the W-B configuration for M=2.30 and M=4.63 are shown in Figs. 8 and 9. It should be observed that the change in the pressure coefficient on the upper surface is smaller when the angle of attack increases, for M=2.30. For M=4.63 no important changes are observed (see Fig. 8).

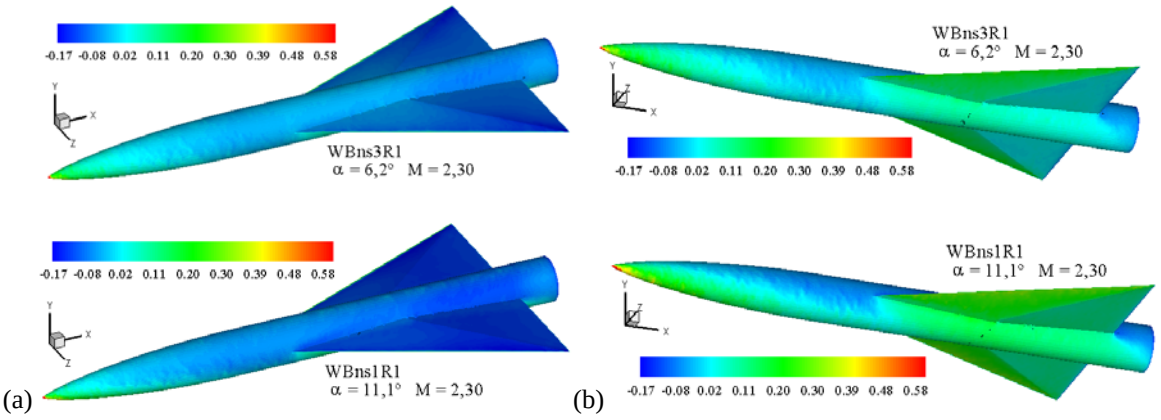

Figure 8. Pressure coefficient distribution over a W-B configuration for M = 2.3 with angle of attack 6.2º and 11.1º. (a) Upper surface, (b) Lower surface

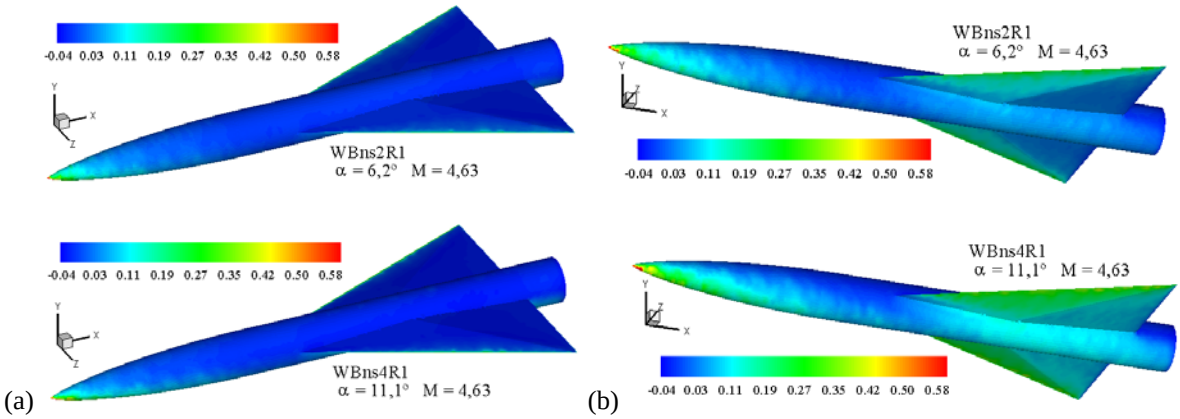

Figure 9. Pressure coefficient distribution over a W-B configuration for M = 4.63 with angle of attack 6.2º and 11.1º. (a) Upper surface, (b) Lower surface

Initially on the lower surface of the wing, the flow is compressed (front region) and later on expanded (rear region) reducing the pressure. The presence of the wing strongly influences the pressure distribution in the body, especially on the lower surface. In the W-B intersection, the pressure coefficient is modified in the leading edge region. It should be noted that the changes are important on the lower surface of the wing because the interaction between the boundary layer of the fuselage and the shock wave of the wing is intense.

Figure 10 shows the meshes and the isolines of Mach numbers in the plane *xy* for different Mach number-angle of attack combinations (all figures use the same Mach number scales for comparative purposes). It can be observed that elements are concentrated in regions where the physical phenomena present high gradients and low velocity. In the forebody region results does not present a good resolution because the mesh does not provide a good transition between the different sizes of elements.

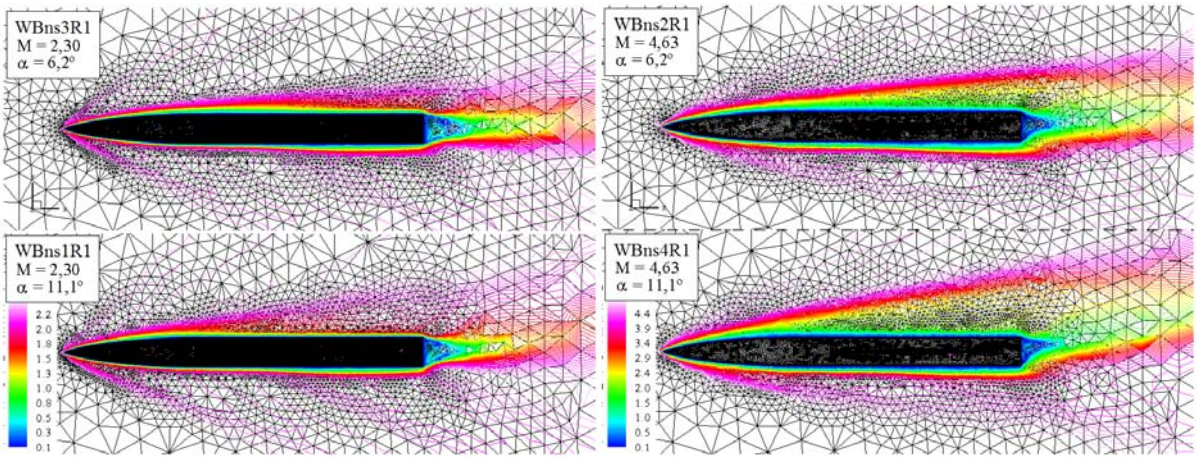

Figure 10. Meshes and Mach number distribution in the symmetric plane over a W-B configuration for M=2.30 and M=4.63 with angle of attack α=6.2º and α=11.1º

Finally, a comparative study of the formation and dynamics of vortices can be seen in Fig. 11 at several longitudinal positions (x_b/L) along the W-B configuration with M=2.30 and M=4.63 and α = 11.1º. The flow field surrounding the W-B configuration is extremely complex, and some features such as multiple vortices influencing the W-B surface pressures are observed. For x_b/L = 0.50, for both Mach numbers, two small vortex on the upper and lower W-B intersection region and a bigger vortex on the upper body region are observed. The size of the vortex over the wing grows for x_b/L=0.80 and x_b/L=0.90; it should be noted that for M=2.30, vortices on the top of the wing and body tend to come together, forming only one vortex. However, for M=4.63 two well defined vortices are observed.

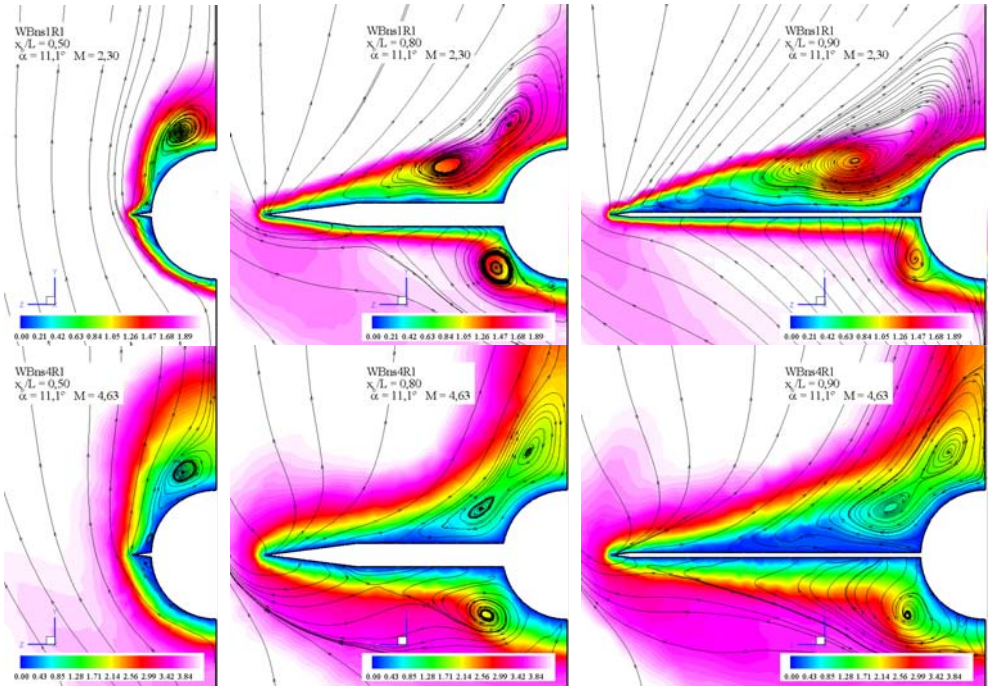

Figure 11. Mach number contours and streamlines in a cross flow plane over a W-B configuration for M=2.30 and 4.63 with angle of attack 11.1º

3.3. Aerodynamic coefficients

The surface pressures computed from the Euler/Navier-Stokes solver are integrated to determine the drag (*CD*), lift (*CL*) and pitching moment (*CMz*) coefficients. Experimental data are not available for this configuration. The aerodynamic coefficients are reported in Tab. 3. It is considered, as reference values, that the coefficients at the wing surface and at the span of the wing. The pitching moment coefficient is taken at coordinates (1.0, 0.0, 0.0).

Table 3. Aerodynamic coefficients for the W-B configuration.

cases	mesh	*CD*	*CL*	*CMz*
M =2.30	WBns3	0.0677	0.293	0.293
α = 6.2º	WBns3R1	0.0597	0.316	0.313
M =2.30 α =11.1º	WBeu1	0.1368	0.563	0.497
	WBeu1R1	0.1492	0.621	0.540
	WBeu1R2	0.1624	0.684	0.566
	WBns1	0.1385	0.516	0.505
	WBns1R1	0.1347	0.549	0.537
M =4.63 α = 6.2º	WBeu2	0.0262	0.170	0.150
	WBns2	0.0463	0.178	0.156
	WBns2R1	0.0591	0.290	0.274
M= 4.63 α =11.1º	WBns4	0.0955	0.336	0.294
	WBns4R1	0.1362	0.528	0.487

The Euler equations predict a slightly higher lift, drag and moment compared to the Navier-Stokes predictions for the case where M=2.30 and α=11.1º, but for the case where M=4.63 and α=6.2º greater values are obtained with the Navier-Stokes equations.

4. CONCLUSIONS

Euler and Navier-Stokes simulations were applied to a wing-body configuration in supersonic regime (M = 2.30 and M = 4.63). These simulations have been performed at moderate angles of attack (α = 6.2º and α = 11.1º) to examine the flow field characteristics, where vortices, shocks and separated flows occurs.

An explicit one-step Taylor-Galerkin scheme (Bono, 2008) has been successfully used to predict the aerodynamic coefficients and flowfields on a wing-body configuration. The solutions with adaptive meshes capture the main flow structure characteristics, as it is demonstrated by comparisons with experimental data. The results of these computations provide valuable insight into the physics of the complex flows around wing-body configurations.

The present study should be extended introducing a turbulence model to accurately predict the effect of Reynolds number in this configuration. This is one of the key areas where CFD can fill a crucial gap in aerodynamic database for any aircraft design effort.

5. ACKNOWLEDGEMENTS

The authors gratefully acknowledge the support of CAPES and CNPq.

6. REFERENCES

Argyris, J., Doltsinis, I.S. and Friz, H., 1990 “Study on computational reentry aerodynamics”, Computer Methods in Applied Mechanics and Engineering, Vol.81, pp. 257–289.

Bono, G., 2008, “Simulação Numérica de Escoamentos em Diferentes Regimes utilizando o Método dos Elementos Finitos” (text in portuguese), Doctoral Thesis, PROMEC, UFRGS, Brazil.

Donea, J., 1984, “A Taylor-Galerkin for convective transport problems”, International Journal for Numerical Methods in Engineering, Vol.20, pp. 101–119.

Jernell, L.S., 1971 “Comparisons of theoretical and experimental pressure distributions over a wing-body model at high supersonic speeds”, TN D-6480, NASA.

Popiolek, T.L. and Awruch, A.M., 2006, “Numerical Simulation of Incompressible Flows using Adaptive Unstructured Meshes and the Pseudo-compressibility Hypothesis”, Advances in Eng. Soft., Vol.37, pp. 260-274.

7. RESPONSIBILITY NOTICE

The authors are the only responsible for the printed material included in this paper.